Research Article | Vol. 27, No. 8 | 15 Apr 2019 | OPTICS EXPRESS 11635
Optics EXPRESS

Design and fabrication of 3-D printed conductive polymer structures for THz polarization control

A. I. HERNANDEZ-SERRANO,[1] QIUSHUO SUN,[2] ELIZABETH G. BISHOP,[3] ELLIOTT R. GRIFFITHS,[3] CHRISTOPHER P. PURSSELL,[3] SIMON J. LEIGH,[3] J. LLOYD-HUGHES,[1] AND EMMA PICKWELL-MACPHERSON[1,2,*]

[1]*Department of Physics, University of Warwick, Gibbet Hill Road, Coventry, CV4 7AL, UK*
[2]*Electronic Engineering, The Chinese Unversity of Hong Kong, Shatin, Hong Kong, China*
[3]*School of Engineering, University of Warwick, Gibbet Hill Road, Coventry, CV4 7AL, UK*
[*]*e.macpherson@warwick.ac.uk*

Abstract: In this paper, we numerically and experimentally demonstrate the inverse polarization effect in three-dimensional (3-D) printed polarizers for the frequency range of 0.5 - 2.7 THz. The polarizers simply consist of 3-D printed strip lines of conductive polylactic acid (CPLA, Proto-Pasta) and do not require a substrate or any further metallic deposition. The experimental and numerical results show that the proposed structure acts as a broadband polarizer between the range of 0.3 THz to 2.7 THz, in which the inverse polarization effect is clearly seen for frequencies above 0.5 THz. In the inverse polarization effect, the transmission of the transverse electric (TE) component exceeds that of the TM component, in contrast to the behavior of a typical wire-grid polarizer. We show how the performance of the polarizers depends on the spacing and thickness of the CPLA structure; extinction ratios higher than 20 dB are achieved. This is the first report using CPLA to fabricate THz polarizers, demonstrating the potential of using conductive polymers to design THz components efficiently and robustly.

1. Introduction

Terahertz (THz) radiation has attracted the attention in a wide range of fields, including, but not limited to, *in vivo* biomedical characterisation [1,2], the automotive industry [3], botanics [4], cultural heritage [5], and materials characterization [6]. Thus, devices able to manipulate THz radiation are in high demand. Unfortunately, the materials used for optical components, for example glass, are opaque at terahertz frequencies. To address this problem, researchers have turned their attention to 3-D printed technology given the low attenuation of some printable plastics in this frequency range [7]. Additionally, the resolution of conventional three-dimensional (3-D) printers is high enough to fabricate components for the THz range (0.4 mm aprox.). Several devices built using this technology have been reported in recent years. Examples include anti-reflective structures [8–10], tunable prisms [11], Bragg fibers [12]. In addition, some new materials have been explored, for example, conductive filaments, used for printed electronic circuits [13]. The conductive properties of these materials are attributed to the mixture of a polymer host and either graphene (Black Magic 3-D) or carbon black (Proto-pasta) [13]. Production of several 3-D printed polarizers has been reported recently [14–16]. Some of these structures printed in plastic are subsequently coated with metallic thin films to improve the performance of the device [14,15]. Super ink-jet printers are able to print complicated metallic structures with comparable accuracy to photolithography [16]. Thus, by printing wire grid patterns on THz transparent substrates such as silicon, super ink-jet printing can be used to fabricate broadband polarizers. In this paper we report, to the best of our knowledge, the first 3-D printed polarizers made of

#359446 https://doi.org/10.1364/OE.27.011635
Journal © 2019 Received 1 Feb 2019; revised 14 Mar 2019; accepted 21 Mar 2019; published 11 Apr 2019

Optics EXPRESS

conductive PLA (proto pasta) with extinction ratios above 20 dB for 0.5 to 1.7 THz. For these polarizers no substrate or metallic coating is needed, improving their robustness and lowering their cost. This approach is more flexible, rapid and robust, and is able to produce polarizers with extinction ratios better than 20dB. Furthermore, given the flexibility of the 3-D printing technique, more exotic polarizers for complex polarization states will be possible using conductive filaments. We also report experimental evidence of the inverse polarization effect and show how it depends on the spacing thickness. In this phenomenon, the transverse electric (TE) component of the radiation is transmitted and the transverse magnetic (TM) component is reflected, opposite to the behavior of a conventional wire-grid polarizer [17–19]. In other words, the transmission efficiency of the TE component exceeds the transmission efficiency of the TM component. In our case, extinction ratios in the inverse region exceed the 20 dB mark. This effect has been reported for the visible range in Cr and Au polarizers [20,21], observing a stronger extinction ratio within the inverse region, even stronger than in the normal region. Additionally, in this work we show a strong relationship between the inverse polarization frequency and the cutoff frequency of a rectangular waveguide. Our experimental results show that below 0.5 THz, the TE component is attenuated while the TM component is transmitted through the device. Conversely, for frequencies above 0.5 THz, the inverse polarization effect dominates the performance increasing the extinction ratio beyond the 20 dB mark. Our experimental results are supported by electromagnetic simulations.

2. Design and fabrication

A simplified diagram of the polarizer is shown in Fig. 1(a). The device consists of 0.3 mm printed strip lines made of conductive PLA, separated by 0.3 mm air gaps (fill factor 50%). This fill factor was chosen to increase the extinction ratio of the polarizer [21]. A photograph of the finished device is shown in Fig. 1(b). Five different polarizers with thicknesses (axial dimension) of 1 mm, 2 mm, 3 mm, 4 mm and 5 mm were printed and tested. The polarizers were fabricated using a 3-D printer built by the Digital and Material Technologies Laboratory at the School of Engineering at the University of Warwick. The resolution of the printer is x = 12.5 μm, y = 12.5 μm and z = 0.625 μm, build volume of 120x120x40 mm, and an Olson Ruby Nozzle with 0.4 mm size was used. Print settings were chosen to give a nozzle temperature of 220°C, bed temperature of 50°C and print speed of 80 mm/s. To retrieve the optical properties of CPLA, a 0.22 mm thick solid disk was printed and tested using THz transmission spectroscopy in a set up similar to the one used by Squires et al. [7]. The refractive index and absorption coefficient of CPLA are shown in Fig. 1(c) and Fig. 1(d), respectively. The absorption coefficient of this material is higher than any other printable plastic tested until now [7]. The highly dispersive behavior of the refractive index is caused by the presence of carbon black in the PLA host.

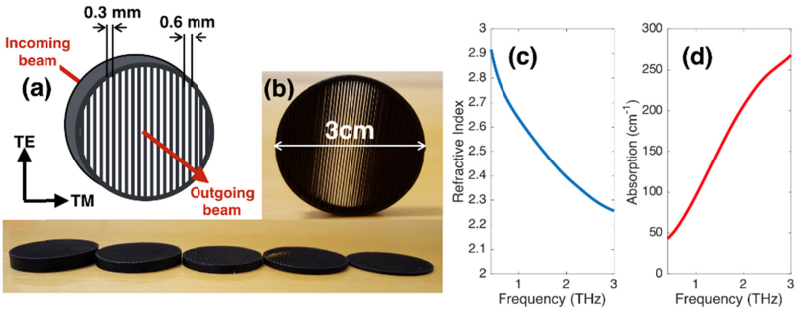

Fig. 1. (a) Diagram of the proposed polarizer; (b) Photograph of the printed devices; (c) and (d) show the refractive index and absorption coefficient of CPLA, respectively.

#359446 https://doi.org/10.1364/OE.27.011635
Journal © 2019 Received 1 Feb 2019; revised 14 Mar 2019; accepted 21 Mar 2019; published 11 Apr 2019

Optics EXPRESS

Commercial finite-element method (FEM) software (COMSOL Multiphysics) was used to verify the operation of the proposed device. We used the electromagnetic waves, frequency domain (ewfd) module. For the simulations we used a collimated Gaussian beam with an amplitude of 1 V/m propagated from the top to the bottom in the simulation space (y-direction). The mesh discretization used in the simulated space was equal to $\lambda/8$ in order to ensure accuracy and scattering boundary conditions were met. Mesh discritizations smaller than this value resulted in no significant improvement in the numerical results (and took longer to process). The material parameters are plotted Figs. 1(c) and 1(d). In Fig. 2, the simulation results are shown for two different frequencies, 0.3 THz and 2.5 THz.

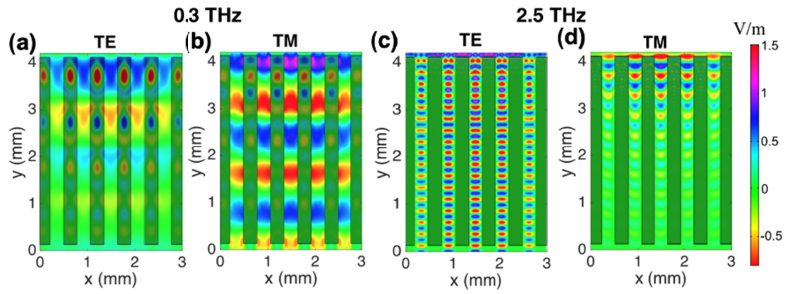

Fig. 2. Numerical simulations for a 4 mm propagation length polarizer. (a) and (b) show the simulation for the TE and TM components of the THz beam at 0.3 THz, respectively; (c) and (d) show the simulation of the TE and TM components at 2.5 THz, respectively. The incoming beam goes from top to bottom. The darkest areas indicate the presence of CPLA, and light green areas indicate air.

In this figure, it is clearly observed that for 0.3 THz, the TE component is highly attenuated in a distance no longer than 2 mm. In contrast, the TM component at the same frequency is transmitted with almost no attenuation, showing the performance of a conventional polarizer. Using effective-medium-theory equations [22], it is straightforward to prove that the effective absorption coefficient of the device for the TE component is almost as high as for the bulk material, contrary to the TM component in which the absorption coefficient is below 5 cm^{-1} for this particular frequency. Furthermore, the simulated results for 2.5 THz show an inversion in the performance of the device. This time the TE component is transmitted but the TM component is highly attenuated. Interestingly, the formation of guided modes in the air gaps is predicted in the simulation for the TE and TM components, similar to those formed inside a metallic rectangular waveguide [23,24].

3. Experimental characterization and results

For the experimental characterization, a Terapulse 4000 from TeraView Ltd THz-TDS spectrometer was used. This device is capable of generating and detecting terahertz radiation in a spectral range from 0.06 THz to 4 THz. The experiments were carried out using transmission geometry [7] and the polarizer was mounted on a rotary holder in order to change the angle between the vertical polarization direction of the incident beam and the strip lines in steps of 10°. This angle was measured with respect to the vertical direction, as shown in the inset of Fig. 3(b). Then, the signal collected by the detector was Fourier transformed in order to extract its spectral content. In Fig. 3, the spectral amplitude and transmission of the recorded THz beam through the 4 mm thick device are shown. In Fig. 3(a), the polarization inversion effect is clearly detected for frequencies above 0.5 THz. Below this frequency, the device acts in the same manner as a traditional polarizer.

The inverse polarization effect has been observed in the visible range in gold and silver strip polarizers [20,21]. In this effect, when the wavelength of the incident light is comparable to the period of the strips, the energy is coupled into the polarizer. This phenomenon is similar to coupling radiation inside a waveguide, enhancing the coupled energy of the TE

#359446 https://doi.org/10.1364/OE.27.011635
Journal © 2019 Received 1 Feb 2019; revised 14 Mar 2019; accepted 21 Mar 2019; published 11 Apr 2019

Optics EXPRESS

modes [21]. For wavelengths larger than the period of the strips, effective-medium theory predicts higher efficiencies for TM components compared to those of the TE components.

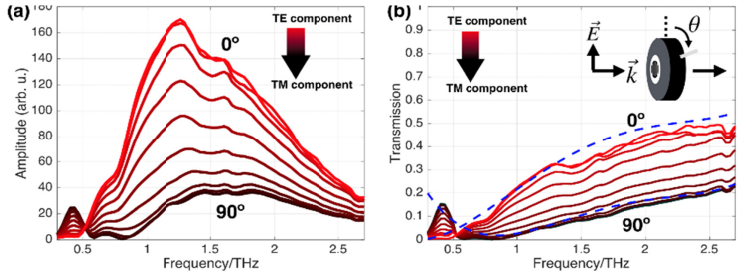

Fig. 3. (a) Spectral content of the THz beam recorded after passing through the 4 mm polarizer and (b) transmission amplitude. The signals were recorded from the case of polarization direction parallel to the strip lines (TE component) to the case of polarization direction perpendicular to the lines (TM component) in steps of 10°. The dashed lines in (b) represent the numerical prediction of the transmission for the TE and TM components.

In Fig. 3(b), the transmission as a function of the frequency for different angles is shown. In the entire range between 0.3 THz and 2.7 THz the transmission is less than 50% which is natural given the 50% fill factor present in the device. Additionally, the transmission reaches 50% for higher frequencies when the incident angle is 0° (TE component) and it falls to 20% for an incident angle of 90° (TM component). The dotted lines in Fig. 3(b) show the numerical results for the transmission. The predictions agree well with the experimental data. The discrepancies at high frequencies are attributed to imperfections of the printed device which will have a significant effect at these frequencies. To further explore the dependency of the inverse polarization effect with the geometrical parameters of the polarizer, five additional polarizers were printed. This time, the spacing between the CPLA strip lines was varied from 0.3mm to 0.7mm keeping the thickness of the devices at 4mm. Only the transmitted amplitudes of the TE and TM components were recorded in this experiment (0° and 90°, respectively). In order to find the frequency at which the inverse effect appears, the ratio between the spectral amplitude of the TE component and the TM component was determined for every polarizer. At the inversion point the amplitudes of both components are equal: the frequency at which this ratio was close to unity was recorded. In Fig. 4, the recorded frequencies are plotted as blue circles. The cut-off frequency of a rectangular waveguide is given by:

$$f_c = \frac{c}{2h} \tag{1}$$

where c is the speed of light in vacuum and h is the spacing between strip lines. This is plotted as a continuous black line in Fig. 4(a) and agrees well with the experimental data thus it is clear that the inversion frequency can be tuned by changing the spacing between strip lines. Additionally, in Fig. 4(b), the extinction ratio of each 0.3 mm spacing polarizer is presented. The extinction ratio was calculated by $20\log(T_{TE}/T_{TM})$, where T_{TE} and T_{TM} are the Fourier transforms of the transmitted radiation at an incident angle of 0° and 90°, respectively. In this figure, a sharp peak for the 4 mm and 5 mm polarizers around 0.8 THz is observed. These abrupt changes in the extinction coefficient correspond to a minimum in the transmittance for the TM component. These peaks are close to the Rayleigh wavelength (dotted line) [15], that is, for this frequency the diffracted beam emerges tangentially to the surface of the polarizer [21]. Furthermore, it is clearly shown that a remarkable improvement in the extinction ratio is achieved by increasing the thickness of the polarizer. Our experimental results show that extinction ratios lower than 20 dB are found for the normal region (below 0.5 THz) while ratios higher than 20 dB are possible for the 4 mm and 5 mm

#359446 https://doi.org/10.1364/OE.27.011635

Received 1 Feb 2019; revised 14 Mar 2019; accepted 21 Mar 2019; published 11 Apr 2019

Optics EXPRESS

polarizers, i.e, the TE component is ten times stronger than the TM component for the 4 mm and 5 mm cases. In addition, Fig. 4(c) shows the transmission of the TE component through the five polarizers. From this figure, it can be concluded that the transmission efficiency goes down as a function of the thickness of the device. This is because ohmic losses are stronger for thicker polarizers given the larger distance the radiation has to travel inside the device. In contrast, the extinction ratio is improved for thicker polarizers (see Fig. 4(b). In conclusion, a compromise between transmission efficiency and extinction ratio has to be made in the design of the polarizer [21].

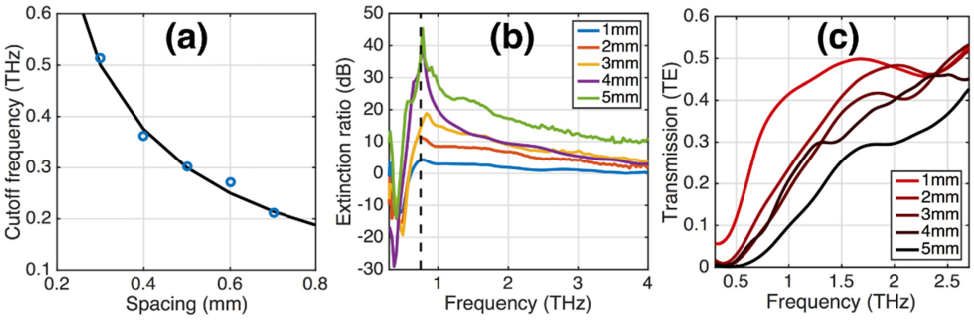

Fig. 4. (a) Cutoff frequency as function of CPLA strip lines separation for the 4 mm thickness. The continuous line is the theoretical cutoff frequency. (b) Extinction ratio of the different polarizers. The dashed line is the predicted Rayleigh wavelength [21]. (c) Transmission of the TE component through the five polarizers.

The time-frequency distributions are shown in Fig. 5 to give more performance information of the proposed device. These distributions were calculated by performing the windowed Fourier transform (Gabor transform) to the THz signals using a sliding Gaussian window with a 1ps standard deviation. The distributions show the arrival time of every frequency at the detector after passing through the 5 mm polarizer.

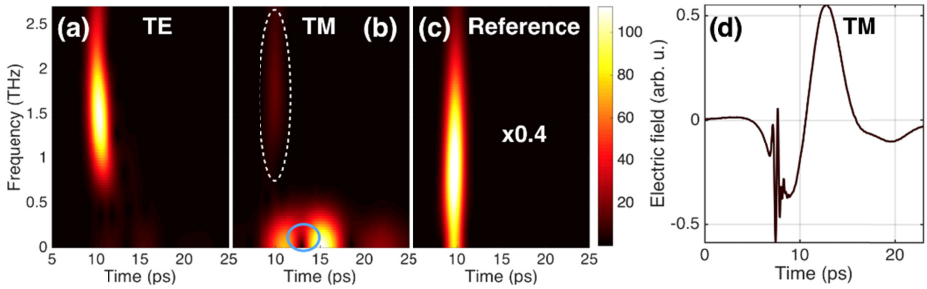

Fig. 5. Time-Frequency distribution of the signal recorder by the receiver for the 5 mm thick polarizer. (a) and (b) show the time-frequency distribution for the TE and TM components respectively. The white dashed circle indicates the remnants of the high frequencies. (c) shows the time-frequency distribution of a reference pulse, that is, without polarizer. The image was scaled 0.4 times. (d) a typical THz pulse waveform after the 5 mm thick polarizer. In this figure, a clear separation between high frequencies and low frequencies is observed.

Figure 5(a) shows that all frequencies above 0.5 THz arrive at the detector at around 9 ps for the TE component, providing experimental evidence that, for these frequencies, the refractive index is almost constant. Conversely, for the TM component, in Fig. 5(b) frequencies above, 0.5 THz are highly attenuated and only frequencies below this value can propagate inside the structure. A rough arrival time of 14 ps is assumed at these low frequency components. An approximation for the refractive index of the TM components results in $n_{TM} = 1.4$, which is in agreement with the calculated results from effective-medium-theory [22]. In Fig. 5(c), the time-frequency distribution for the reference pulse is also shown.

#359446 https://doi.org/10.1364/OE.27.011635
Journal © 2019 Received 1 Feb 2019; revised 14 Mar 2019; accepted 21 Mar 2019; published 11 Apr 2019

Optics EXPRESS

As expected all frequencies arrive at the same time, around 9 ps. Comparing this arrival time with the arrival time for frequencies in the TE component (Fig. 5(a)), we can conclude that the refractive index for the TE components above 0.5 THz is around 1. This value is again confirmed using effective-medium-theory equations [22] and is in agreement with the FEM simulation results at 2.5 THz (Fig. 2). Finally, a typical waveform for the TM component is shown in Fig. 5(d). The rapid oscillations of the THz pulse between 5 and 10 ps in Fig. 5(d) are due to the high frequency components that leaked through the polarizer. These high frequency components are shown in Fig. 5(b) as a slightly red area around 10ps for frequencies from 0.5THz to 2.7 THz (circled in white). From Fig. 5(d), it is clear that the amplitude of the THz pulse near to 11ps is zero, consequently, when the Gaussian window (1ps standard deviation) is multiplied by that region the resulting Gabor transform vanishes. This explains the black spot in Fig. 5(b) in the TM frequency-time distribution (circled in blue). By taking a wider Gaussian window, more non-zeros amplitude values will be enclosed by the window eliminating this black region, but with the cost of losing certainty in the arrival time of every frequency.

4. Conclusion

In conclusion, we have shown that it is possible to fabricate functional polarizers for a wide range of frequencies in the THz range by printing strip lines of conductive PLA (proto-pasta). In this work we printed 3cm diameter polarizers made of 0.3 mm strip depositions of conductive PLA separated by 0.3 mm air gaps. We printed five different polarizers with different thickness from 1 mm to 5 mm. The best performance was found with the 5 mm thick polarizer. In addition, we demonstrated the inverse polarization effect in a 3-D printed polarizer for frequencies above 0.5 THz. This frequency matches with the cut-off frequency calculated for a metallic rectangular waveguide with the same dimensions. This type of printed device is quick and easy to fabricate, mechanically robust and additionally low cost, making it an invaluable addition for future THz components for communication and imaging applications.

Funding

Hong Kong PhD Fellowship Scheme; Royal Society Wolfson Merit Award; Royal Society research grant (RG100120); School of Engineering at the University of Warwick; and EPSRC project EP/N010825/1.

References

1. Q. Sun, E. P. J. Parrott, Y. He, and E. Pickwell-MacPherson, "In vivo thz imaging of human skin: Accounting for occlusion effects," J. Biophotonics **11**(2), e201700111 (2018).
2. G. G. Hernandez-Cardoso, S. C. Rojas-Landeros, M. Alfaro-Gomez, A. I. Hernandez-Serrano, I. Salas-Gutierrez, E. Lemus-Bedolla, A. R. Castillo-Guzman, H. L. Lopez-Lemus, and E. Castro-Camus, "Terahertz imaging for early screening of diabetic foot syndrome: A proof of concept," Sci. Rep. **7**(1), 42124 (2017).
3. S. Krimi, J. Klier, J. Jonuscheit, G. von Freymann, R. Urbansky, and R. Beigang, "Highly accurate thickness measurement of multi-layered automotive paints using terahertz technology," Appl. Phys. Lett. **109**(2), 021105 (2016).
4. E. Castro-Camus, M. Palomar, and A. A. Covarrubias, "Leaf water dynamics of Arabidopsis thaliana monitored in-vivo using terahertz time-domain spectroscopy," Sci. Rep. **3**(1), 2910 (2013).
5. J. Cacciari and S. Siano, "Use of thz reflectometry for rouhness estimations of archeoloical metal surfaces," J. Infrared Millim. Terahertz Waves **38**(4), 503–517 (2017).
6. Q. Sun, X. Liu, J. Cao, R. I. Stantchev, Y. Zhou, X. Chen, E. P. Parrott, J. Lloyd-Hughes,N. Zhao, and E. Pickwell-MacPherson, "Highly sensitive terahertz thin-film total internal reflection spectroscopy reveals in situ photoinduced structural changes in methylammonium lead halide preovskites," J. Phys. Chem. C **122**, 17552–17558 (2018).
7. A. Squires and R. Lewis, "Feasibility and characterization of common and exotic filaments for use in 3-D printed terahertz devices," J. Infrared Millim. Terahertz Waves **39**(7), 614 (2018).
8. J. Bomba, J. Suszek, M. Makowski, A. Sobczyk, and M. Sypek, "3-d printed anti-reflection structures for the terahertz region," J. Infrared Millim. Terahertz Waves **39**(1), 24–35 (2018).

#359446 https://doi.org/10.1364/OE.27.011635
Journal © 2019 Received 1 Feb 2019; revised 14 Mar 2019; accepted 21 Mar 2019; published 11 Apr 2019

Optics EXPRESS

9. H. Xin and M. Liang, "3-D printed microwave and THz devices using polymer jetting techniques," Proc. IEEE **105**(4), 737–755 (2017).
10. D. Jahn, R. Eckstein, L. M. Schneider, N. Born, G. Hernandez-Sosa, J. C. Balzer, I. Al-Naib, U. Lemmer, and M. Koch, "Digital aerosol jet printing for the fabrication of terahertz metamaterials," Advanced Materials Technologies **3**(2), 1700236 (2018).
11. S. F. Busch, E. Castro-Camus, F. Beltran-Mejia, J. C. Balzer, and M. Koch, "3d printed prisms with tunable dispersion for the thz frequency range," J. Infrared Millim. Terahertz Waves **39**(6), 553–560 (2018).
12. J. Li, K. Nallappan, H. Guerboukha, and M. Skorobogatiy, "3-D printed hollow core terahertz Bragg waveguides with defect layers for surface sensing applications," Opt. Express **25**(4), 4126–4144 (2017).
13. P. F. Flowers, C. Reyes, S. Ye, M. J. Kim, and B. J. Wiley, "3-D printing electronic components and circuits with conductive thermoplastic filament," Additive Manufacturing **18**, 156–163 (2017).
14. A. Macor, E. de Rijk, S. Alberti, T. Goodman, and J.-P. Ansermet, "Note: Three-dimensional stereolithography for millimeter wave and terahertz applications," Rev. Sci. Instrum. **83**(4), 046103 (2012).
15. M. Ryu, D. Linklater, W. Hart, A. Balcytis, E. Skliutas, M. Malinauskas, D. Appadoo, Y.-R. E. Tan, E. P. Ivanova, J. Morikawa, and S. Juodkazis, "3-D printed polarizing grids for IR-THz synchrotron radiation," J. Opt. **20**(3), 035101 (2018).
16. K. Takano, T. Kawabata, C.-F. Hsieh, K. Akiyama, F. Miyamaru, Y. Abe, Y. Tokuda, R.-P. Pan, C.-L. Pan, and M. Hangyo, "Fabrication of terahertz planar metamaterials using a super-fine ink-jet printer," Appl. Phys. Express **3**(1), 016701 (2010).
17. G. R. Fowles, *Introduction to Modern Optics* (Courier Corporation, 1989).
18. K. Imakita, T. Kamada, M. Fujii, K. Aoki, M. Mizuhata, and S. Hayashi, "Terahertz wire grid polarizer fabricated by imprinting porous silicon," Opt. Lett. **38**(23), 5067–5070 (2013).
19. C. D. W. Mosley, M. Failla, D. Prabhakaran, and J. Lloyd-Hughes, "Terahertz spectroscopy of anisotropic materials using beams with rotatable polarization," Sci. Rep. **7**(1), 12337 (2017).
20. M. Honkanen, V. Kettunen, M. Kuittinen, J. Lautanen, J. Turunen, B. Schnabel, and F. Wyrowski, "Inverse metal-stripe polarizers," Appl. Phys. B **68**(1), 81–85 (1999).
21. A. Drauschke, B. Schnabel, and F. Wyrowski, "Comment on the inverse polarization effect in metal-stripe polarizers," J. Opt. A, Pure Appl. Opt. **3**(1), 67–71 (2001).
22. M. Scheller, C. Jördens, and M. Koch, "Terahertz form birefringence," Opt. Express **18**(10), 10137–10142 (2010).
23. A. I. Hernandez-Serrano, R. Mendis, K. S. Reichel, W. Zhang, E. Castro-Camus, and D. M. Mittleman, "Artificial dielectric stepped-refractive-index lens for the terahertz region," Opt. Express **26**(3), 3702–3708 (2018).
24. R. Mendis and D. M. Mittleman, "Comparison of the lowest-order transverse-electric (TE1) and transverse-magnetic (TEM) modes of the parallel-plate waveguide for terahertz pulse applications," Opt. Express **17**(17), 14839–14850 (2009).

#359446 https://doi.org/10.1364/OE.27.011635
Journal © 2019 Received 1 Feb 2019; revised 14 Mar 2019; accepted 21 Mar 2019; published 11 Apr 2019